Input-specific maturation of synaptic dynamics of parvalbumin interneurons in primary visual cortex

Jiangteng Lu[a], Jason Tucciarone[a,b,c], Ying Lin[a], and Z. Josh Huang[a,1]

[a]Cold Spring Harbor Laboratory, Cold Spring Harbor, NY 11724; and [b]Medical Scientist Training Program and [c]Program in Neuroscience, Stony Brook University, Stony Brook, NY 11790

Cortical networks consist of local recurrent circuits and long-range pathways from other brain areas. Parvalbumin-positive interneurons (PVNs) regulate the dynamic operation of local ensembles as well as the temporal precision of afferent signals. The synaptic recruitment of PVNs that support these circuit operations is not well-understood. Here we demonstrate that the synaptic dynamics of PVN recruitment in mouse visual cortex are customized according to input source with distinct maturation profiles. Whereas the long-range inputs to PVNs show strong short-term depression throughout postnatal maturation, local inputs from nearby pyramidal neurons progressively lose such depression. This enhanced local recruitment depends on PVN-mediated reciprocal inhibition and results from both pre- and postsynaptic mechanisms, including calcium-permeable AMPA receptors at PVN postsynaptic sites. Although short-term depression of long-range inputs is well-suited for afferent signal detection, the robust dynamics of local inputs may facilitate rapid and proportional PVN recruitment in regulating local circuit operations.

input-specific | short-term plasticity | synapse | parvalbumin interneuron | maturation

GABAergic inhibitory interneurons are essential components of cortical circuitry. They regulate the balance and rapid spatiotemporal configuration of neural ensembles for information coding, processing, and propagation (1, 2). Among the diverse classes of interneurons, parvalbumin-positive interneurons (PVNs) mediate inhibition of the perisomatic region of pyramidal neurons (PyNs). Both intrinsic properties and synaptic output of PVNs are characterized by speed and reliability, facilitating a rapid conversion of excitatory input to inhibitory output (3, 4). These physiological characteristics allow PVNs to regulate the temporal precision of afferent signals and the dynamic operation of pyramidal networks (5, 6). PVNs of primary visual cortex (V1) form extensive recurrent connections with PyNs of the same layer (7, 8), and further receive long-range excitatory inputs from other layers (7) and other brain areas. Depending on the input source, PVNs mediate both feedback and feedforward inhibition. Direct optogenetic activation of PVNs strongly modulates PyN spiking and gain control during visual processing and generates synchronizing gamma oscillations (9, 10). However, the synaptic properties of the physiological recruitment of PVNs to initiate either feedforward or feedback inhibition are not fully understood. Several studies demonstrate significant developmental maturation in the intrinsic properties, inhibitory transmission, and innervation patterns of PVNs in mouse V1 after eye opening (11, 12). Whether long-range and local recruitment of PVNs undergo such developmental maturation is unknown.

Here we systematically mapped the sources of long-range inputs to PVNs in mouse V1 and then investigated local (same laminar) and long-range (other cortical and subcortical sources) excitatory inputs to PVNs in V1 layer 2/3 (L2/3) from juvenile to adult ages. We found input-specific maturation of short-term synaptic dynamics of these PVNs, depending on the maturation of PVN-mediated reciprocal inhibition of PyNs.

Results

Long-Range Inputs to V1 PVNs. We first investigated sources of input to V1 PVNs using rabies virus monosynaptic tracing (13, 14) (Fig. S1*A*). As expected, dense local PyNs form synapses onto V1 PVNs (Fig. S1*C*). In addition to lateral geniculate nucleus (LGN), secondary visual cortex (V2), primary auditory (A1) and somatosensory (S1) areas, premotor area (M2), and contralateral cortex (CC) are among the major input sources (Fig. S1 *D* and *E*). Thus, V1 PVNs can be recruited by local excitatory inputs from nearby PyNs and long-range excitatory inputs from multiple brain regions (Fig. S1*F*).

Differential Synaptic Dynamics at Local and Long-Range Inputs to L2/3 PVNs in Mature V1. To validate the rabies tracing results and physiologically characterize long-range and local inputs to L2/3 PVNs, we used channelrhodopsin 2 (ChR2)-assisted circuit mapping (CRACM) in parvalbumin-*ires-Cre*:Ai9 mice (containing the *Rosa26-loxpSTOPloxp-tdTomato* allele; SI Materials and Methods). We virally delivered ChR2 to ipsilateral M2 to test the M2 input (Fig. 1*A*). We used in utero electroporation to express ChR2 in L2/3 PyNs in one cortical hemisphere; this allowed us to test the CC input, or the intralaminar input, from L2/3 PyNs when we recorded PVNs in the ChR2-expressing V1 (Fig. 1*B*). We studied these three inputs to L2/3 PVNs from 5- to 8-wk-old mice. Monosynaptic responses were measured in both M2 and CC input (Fig. 1 *A* and *B*), suggesting that other long-range sources revealed by rabies tracing (Fig. S1) are likely physiologically relevant. We then examined short-term synaptic dynamics by paired light stimulation (Fig. 1 *A–C*). Both long-range inputs showed strong

Significance

Proper recruitment of inhibitory interneurons is crucial to configuring cortical neural circuits for information processing and propagation, but the development of synaptic inputs to these interneurons is not well-understood. We traced the sources of long-range and local inputs to a major interneuron subtype, the-parvalbumin-positive interneurons (PVNs), in mouse visual cortex. Whereas the long-range inputs show strong short-term synaptic depression, local recurrent inputs gradually lose such depression during postnatal maturation. We further uncovered the circuitry and molecular mechanisms that contribute to this source-dependent maturation in synaptic inputs. Although short-term depression of long-range inputs is well-suited for afferent signal detection, the robust synaptic dynamics of local inputs may facilitate rapid and proportional PVN recruitment for regulating network operations.
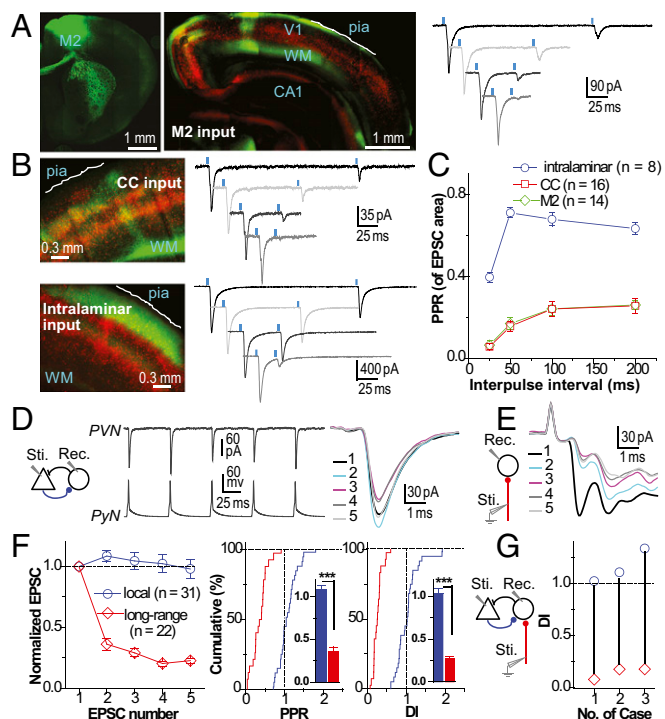
NEUROSCIENCE

Fig. 1. Distinct synaptic dynamics at local and long-range inputs to L2/3 PVNs in V1. (*A, Left*) Adeno-associated virus (AAV)-ChR-GFP injection at M2 and the axons of M2 PyNs transduced by AAV-ChR-GFP projected to V1, in which PVNs express RFP. pia, the top of layer 1; WM, white matter. (*Right*) Sample monosynaptic EPSCs in an L2/3 PVN evoked by paired-pulse light stimulation (488 nm, 1–2 ms, indicated as short blue bars, bath-applied with 1 μM TTX, a sodium channel blocker, and 1 mM 4-AP, a potassium channel blocker) at 200-, 100-, 50-, and 25-ms intervals from top to bottom, averaged from 10–20 trials. (*B, Left*) Contralateral (*Upper*) and intralaminar input (*Lower*) to L2/3 PVNs. (*Right*) Same as A, Right. (*C*) Summary of PPR of the intralaminar input and two long-range inputs to PVNs. Rec., postsynaptic recording; Sti., presynaptic stimulation. (*D, Left*) Schematic of whole-cell patch recording of local PyN input to PVN. (*Center*) Sample EPSCs in a PVN evoked by a train of APs in a presynaptic PyN, averaged from 20 trials. (*Right*) Magnified EPSCs shown (*Center*) aligned to the peak of presynaptic APs. (*E, Left*) Schematic of the recording configuration of long-range input to PVNs. (*Right*) EPSCs were evoked by single-fiber stimulation (0.2 ms, 15 μA, 20 Hz) at L5/6 below the recorded L2/3 PVN, where a monosynaptic EPSC was followed by polysynaptic events; the four consecutively evoked responses were aligned to the first one with the stimulus artifact. (*F, Left*) Summary of short-term dynamics of two inputs, which were normalized to the first EPSC amplitude. (*Center* and *Right*) Comparison of PPR and DI between two inputs as cumulative distribution and mean value in the histograms (*Insets*). (Error bars represent SEM; ***P < 0.001, Mann–Whitney test.) (*G, Left*) Schematic of simultaneous detection of one local input and one long-range input onto the same PVN. (*Right*) DIs for three pairs of converging local (blue circles) and long-range (red diamonds) inputs are aligned for direct comparison.

short-term depression. Paired-pulse ratios (PPRs; response#2/#1 charge) at 25-, 50-, 100-, and 200-ms intervals for M2 inputs (*n* = 14) were 0.07 ± 0.02, 0.17 ± 0.03, 0.24 ± 0.04, and 0.26 ± 0.02, and for CC inputs (*n* = 16) were 0.06 ± 0.01, 0.16 ± 0.03, 0.24 ± 0.04, and 0.26 ± 0.04. In contrast, intralaminar inputs showed much less depression (PPR, 0.40 ± 0.02, 0.71 ± 0.02, 0.68 ± 0.03, 0.63 ± 0.03, *n* = 8), suggesting distinct short-term plasticity compared with long-range inputs.

Because optical stimulation of ChR2 produces stronger synaptic depression (15), we used electrical stimulation to examine the short-term plasticity of excitatory inputs to PVNs. We examined local inputs by unitary synapses to PVNs from nearby PyNs (soma distance less than 100 μm) with multiple whole-cell patch recordings. In comparison, long-range unitary synapses

were examined with single-fiber stimulation applied in L5/6 beneath targeted L2/3 PVNs (Fig. S2), although the exact input source was not identified. In mature V1 (>P30; P, postnatal day), the synaptic strength (the amplitude of unitary excitatory postsynaptic current; uEPSC) was larger in long-range inputs (220.8 ± 31.2 pA, *n* = 26) than in local inputs (114.7 ± 18.7 pA, *n* = 61; *P* < 0.001; Table S1). To examine synaptic dynamics, five consecutive EPSCs in PVNs were evoked by action potentials (APs) in presynaptic PyNs or by repetitive stimulation in ascending fibers. Substantiating the CRACM results, we found no depression in local inputs (PPR, 1.09 ± 0.05; DI, 1.03 ± 0.06; *n* = 31; DI, dynamics index: the mean amplitude of EPSC 2–5 normalized to that of EPSC 1) and strong depression in long-range inputs (PPR, 0.36 ± 0.05; DI, 0.27 ± 0.03; *n* = 22) (Fig. 1 *D–F*).

Although single-fiber stimulation evoked unitary monosynaptic responses and polysynaptic responses (Fig. 2*E*), these polysynaptic events had no impact on monosynaptic depression (Fig. S2). Such depression manifest in broad ranges of frequencies (Fig. S3). The possible contribution of presynaptic inhibition to such depression was excluded, because blocking GABA transmission did not affect long-range input dynamics (Fig. S4). The differences between long-range and local inputs were not caused by different innervation of PVN subclasses: simultaneous recording of pairs of local and long-range inputs converging onto the same PVNs confirmed responses at the level of individual PVNs in mature V1 (Fig. 1*G*).

Distinct Postnatal Maturation Profile in Synaptic Dynamics Between Local and Long-Range Inputs. In contrast to mature V1, previous studies in juvenile rat cortex showed that local inputs to PVNs exhibited short-term depression (16, 17). Thus, we measured the short-term dynamics of both local and long-range inputs in juvenile mice (from P13 to P19). Consistent with previous findings, both inputs showed similar strong depression (local: DI, 0.35 ± 0.02, *n* = 25; long-range: DI, 0.32 ± 0.02, *n* = 21; *P* = 0.63) (Fig. 2 *A–C*). We also observed a strong short-term depression of intralaminar inputs to L2/3 PVNs at juvenile ages (Fig. S5).

Throughout development, depression at local inputs progressively decreased (DI, 0.70 ± 0.05, *n* = 13 in P23–P25) and was lost by P30 (DI, 0.98 ± 0.06, *n* = 12 in P29–P33 mice). There was slight facilitation beyond P42 (P42–P115; DI, 1.06 ± 0.09, *n* = 19; but no significant difference was detected between two later stages, *P* = 0.50) (Fig. 2*D*). These results reveal restricted time windows (from P20 to P29) for maturation of local input dynamics. The loss of depression at mature local inputs includes
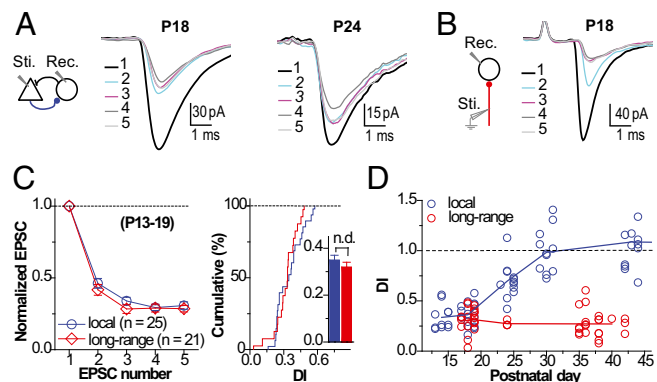

Fig. 2. Progressively enhanced dynamics of local inputs to V1 L2/3 PVNs. (*A* and *B*) The same recording configurations as shown in *D* and *E* at the indicated ages. (*C, Left*) Summary of short-term dynamics of two inputs. (*Right*) Comparison of DI between two inputs as cumulative distribution and mean value in the histogram (*Inset*) (Error bars represent SEM; n.d., no significant difference). (*D*) DI of individual inputs plotted according to their corresponding postnatal age and mean values at each age are linked by a line.

a broad range of frequencies (Fig. S6). Importantly, this change is specific to PVNs, because no such change was detected at PyN-to-PyN synapses (Fig. S7).

In contrast, long-range input to L2/3 PVNs maintained strong depression throughout P13–P44 (P24: DI, 0.27 ± 0.01, n = 4; P35–P44: DI, 0.27 ± 0.02, n = 22) (Fig. 2 B–D). In addition, no significant change was detected in the uEPSC strength in either local or long-range inputs from juvenile to mature ages (Table S1).

Maturation of PVN-Mediated Inhibition Is Necessary for the Enhancement of Local Input Dynamics. A fundamental difference between local and long-range excitatory inputs is the connectivity between their sources and targeted PVNs. PVNs form extensive reciprocal inhibitory synapses to nearby PyNs, which generate local excitatory inputs (thereby completing a PyN⇄PVN loop), but not to distant neurons. We hypothesized that this reciprocal inhibition enhances local input dynamics.

To test this, we examined PVN→PyN connections during postnatal development (Fig. 3 A–C). The strength of individual PVN→PyN synapses, measured as unitary inhibitory postsynaptic current (uIPSC), increased from 43.2 ± 8.9 pA at P13–P14 to 98.8 ± 20.3 pA at P23–P25 (P = 0.015) and then remained stable (94.2 ± 18.6 pA at P29–P33; P = 0.97 vs. at P23–P25) (Fig. 3B). This was largely attributed to increases of α1-subunit–containing GABAa receptors (α1-GABAaRs), an interpretation supported by progressively faster kinetics of inhibitory synaptic responses (uIPSC decay from 5.10 ± 0.32 to 2.32 ± 0.11 ms; P < 0.001) (Fig. 3B) and the stronger effect of zolpidem, an allosteric modulator of α1-GABAaRs, in mature ages (Fig. 3C). Such maturation of PVN-mediated inhibition is also observed in hippocampal basket cells (18). Therefore, the maturation of PVN-mediated inhibitory transmission (plateaus at ~P25) precedes the maturation of synaptic dynamics of local inputs to PVNs (plateaus at ~P30; Fig. 2D).

We sorted a population of unidirectional local inputs without PVN-mediated reciprocal inhibition (~29%; 32 PyN→PVN vs. 79 PyN⇄PVN in one set of experiments). During development we found more PyN⇄PVN than PyN→PVN (Fig. 3A). No detectable difference was found in basal transmission between these two types of local inputs (Table S2). Importantly, whereas the two types of local inputs showed similar depression at juvenile ages (P13–P19; PyN→PVN: DI, 0.39 ± 0.05, n = 10; PyN⇄PVN: DI, 0.47 ± 0.04, n = 17; P = 0.23), the developmental enhancement of synaptic dynamics in PyN→PVN was less in PyN⇄PVN (P30–P115; DI, 0.76 ± 0.05, n = 13 vs. 0.98 ± 0.05, n = 29; P = 0.008) (Fig. 3 D and E). Thus, the presence of reciprocal inhibition correlates with the developmental enhancement of local input dynamics to PVNs.

Furthermore, we selectively reduced the α1-subunit in PyNs using a short hairpin (sh)RNA to α1 (Figs. S8 and S9) delivered to L2/3 PyNs via in utero electroporation at embryonic day (E)15. Approximately 10–20% of L2/3 PyNs in V1 were transfected. At mature ages, PVN-mediated inhibition of PyNs with α1 knockdown was dramatically decreased compared with "naïve neighbor" PyNs without shRNA or those with scramble shRNA. α1 knockdown reduced both the strength (uIPSC amplitude: shRNA-PyN, 33.3 ± 8.0 pA, n = 12; naïve neighbor, 75.7 ± 13.7 pA, n = 10; scramble RNA-PyN, 94.4 ± 21.2 pA, n = 12; P = 0.011 and 0.019 vs. naïve and scramble groups, respectively) and kinetics (uIPSC decay: shRNA-PyN, 3.47 ± 0.40 ms; naïve neighbor, 2.12 ± 0.15 ms; scramble RNA-PyN, 2.26 ± 0.16 ms; P = 0.006 and 0.010 vs. naïve and scramble groups, respectively) of PVN-to-PyN synapses (Fig. 4 A and B). We then examined local input dynamics at mature ages. In PyN⇄PVN (Fig. 4 C and D), local inputs from α1-knockdown PyNs (i.e., with reduced reciprocal inhibition) showed significant depression similar to those at juvenile ages (DI from scramble shRNA-PyN, 1.01 ± 0.05, n = 8; naïve neighbor, 1.06 ± 0.08, n = 11; shRNA-PyN, 0.57 ± 0.04, n = 9; naïve vs. scramble RNA, P = 0.68; shRNA vs.
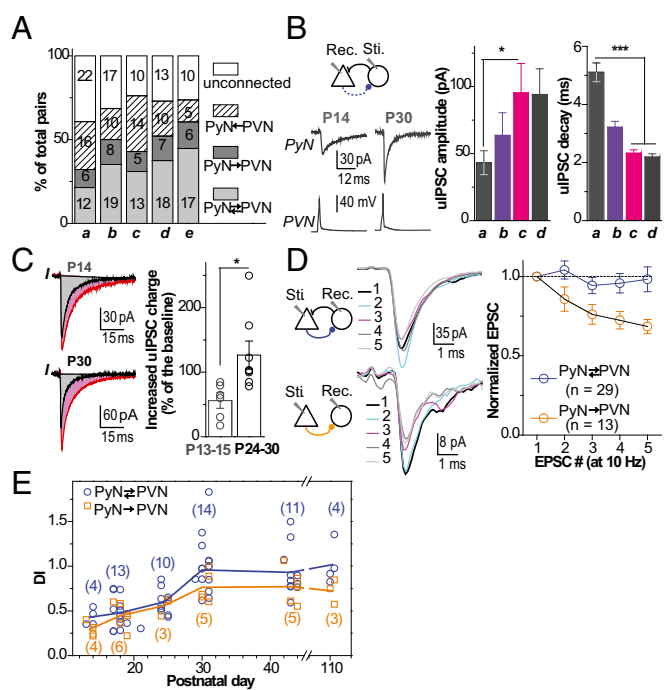

Fig. 3. Maturation of synaptic connectivity between PyN and PVN correlates with the maturation of local input dynamics to PVNs. (A) Distributions of the connectivity patterns in PyN and PVN pairs in V1 L2/3 were plotted as the fraction of total pairs at each age (a, P13–P14; b, P17–P19; c, P23–P25; d, P29–P33; e, >P40) with pair numbers in the corresponding bar. (B, Left) Schematic of the recording configuration; uIPSCs in a PyN evoked by single APs in a PVN at the indicated ages, each trace averaged from 30–50 trials. (Center and Right) Comparison of uIPSC amplitude and decay time among age groups (n = 23, 16, 17, and 17 at ages a–d shown in A, respectively). (Error bars represent SEM; *P < 0.05, ***P < 0.001, Mann–Whitney test.) (C, Left) Samples showing the effect on uIPSCs before (black) and during (red) zolpidem application (0.4 μM) at the indicated ages, each trace averaged from 20–40 trials. (Right) Plot of individual cases (open circles) and summaries (bars) of zolpidem-induced change in IPSC charge transfer (red areas vs. gray area shown; Left). A stronger effect was seen at the more mature age: 56.0 ± 12.0% (P13–P15; n = 6) vs. 126 ± 21.7% (P24–P30; n = 8). (Error bars represent SEM; *P = 0.017; Student t test.) (D, Left) Sample EPSCs in a PVN evoked by 10-Hz APs in a presynaptic PyN at either a PyN⇄PVN (Upper) or PyN→PVN (Lower) pair at mature ages. (Right) Summary of synaptic dynamics of the two types of local inputs at mature ages. (E) DI of individual inputs was plotted and mean values at each age are linked by lines with corresponding colors; the number of connections at each age is indicated. DI values (P13–P14, P17–P19, P24–P25, P30–P31, P42–P44, and P110–P111) for PyN⇄PVN, 0.43 ± 0.05, 0.48 ± 0.05, 0.60 ± 0.05, 0.96 ± 0.09, 0.93 ± 0.08, and 1.02 ± 0.13, and for PyN→PVN, 0.29 ± 0.05, 0.45 ± 0.06, 0.56 ± 0.07, 0.76 ± 0.08, 0.77 ± 0.10, and 0.72 ± 0.10, respectively.

either naïve or scramble RNA, P < 0.001; Student t test). In unidirectional PyN→PVN (Fig. 4 E and F), local inputs initiated from either α1-knockdown PyNs or naïve neighbors showed strong depression (DI from scramble shRNA-PyN, 0.92 ± 0.08, n = 4; naïve neighbors, 0.57 ± 0.06, n = 8; shRNA-PyN, 0.57 ± 0.05, n = 9; naïve vs. shRNA, P = 0.99; both to scramble group, P < 0.01; Student t test). These results indicate that the enhancement of PyN→PVN input dynamics is more sensitive to reduced PVN-mediated inhibition, suggesting that PVN-mediated inhibition may promote cooperation among neighboring PyNs in synergistically enhancing synaptic dynamics to PVNs.

Both Pre- and Postsynaptic Mechanisms Contribute to the Enhanced Dynamics of Local Inputs to PVNs. Short-term synaptic dynamics is modified at presynaptic and/or postsynaptic sites (19). The strong depression of local inputs to PVNs in juvenile cortex correlates
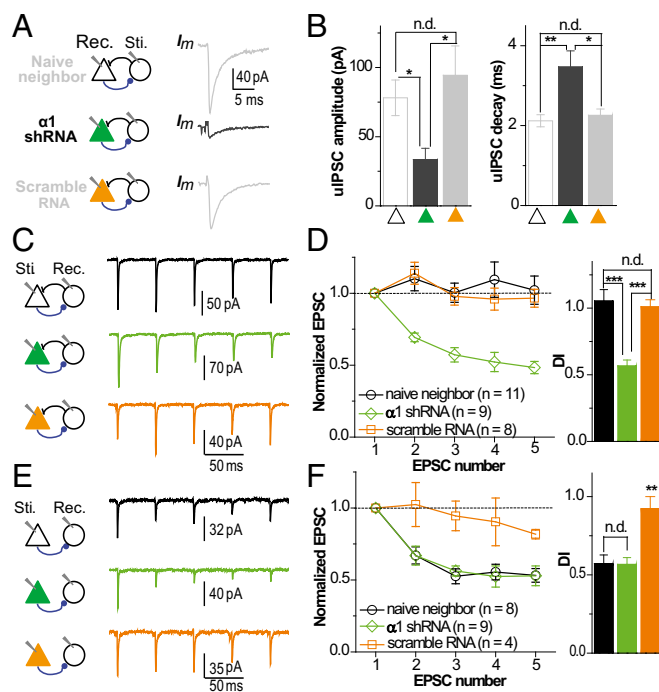
Fig. 4. Sufficient PVN-mediated inhibition is necessary for the maturation of local input dynamics. (A) Examples of uIPSCs recorded in the three conditions illustrated by the schematics. (B) Summaries of uIPSC amplitude and decay times in the three conditions as indicated (A) at P31–P35. The naïve neighbor group and shRNA group were examined in the same preparation. (C and D) Short-term dynamics of local inputs in PyN⇌PVN at mature ages (P31–P35) in the three conditions as in A. Examples of EPSCs (C) were averaged from 20 trials. Summaries of synaptic dynamics and DI (D). (E and F) Short-term dynamics of local inputs in PyN→PVN. Sample EPSCs, summary plot, and graph are as described for C and D. (Error bars represent SEM; *P < 0.05, **P < 0.01, ***P < 0.001, Mann–Whitney test.)

tested the contribution of CP-AMPARs by examining the current–voltage (I–V) relationship of isolated AMPAR-mediated EPSCs at both local and long-range inputs before and after P20–P29. The extent of inward rectification inversely correlated with the normalized uEPSC amplitude at a +70 mV holding potential of PVNs, with significantly larger reductions at local inputs (from 0.48 ± 0.03 at P17–P19 to 0.23 ± 0.02 at P32–P34, $P < 0.001$; Student t test) (Fig. 5A) than at long-range inputs (from 0.51 ± 0.07 at P17–P19 to 0.48 ± 0.04 at P31–P33, $P = 0.28$; Student t test) (Fig. 5B). Furthermore, blocking CP-AMPARs by application of NAS (1-naphthyl acetyl spermine, a selective antagonist of CP-AMPARs; 100 μM) had stronger effects on basal transmission of local input synapses at mature vs. young ages (Fig. 5C and Fig. S12). Thus, both larger inward rectification and stronger NAS effect on synaptic transmission showed a developmentally increased ratio of CP-AMPAR to Ca^{2+}-impermeable AMPAR expression in local inputs to PVNs. Given the increase of total postsynaptic receptors (Fig. S11), together these results suggest increased CP-AMPAR expression at local input synapses.

NAS application dramatically reduced synaptic dynamics of local inputs at mature ages (DI: from 0.97 ± 0.06 to 0.66 ± 0.04, $n = 14$, $P < 0.001$; Student's paired t test) but slightly at young ages (DI:
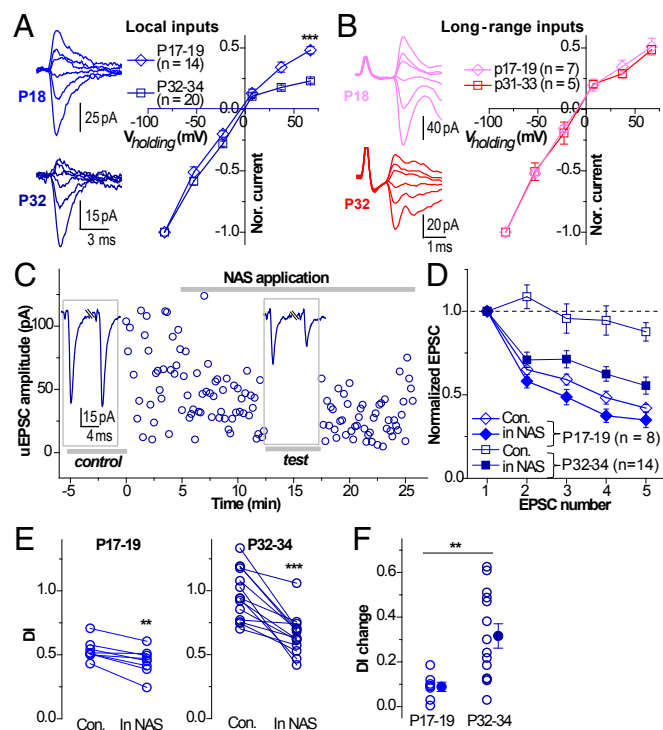

Fig. 5. Input-specific increase of postsynaptic CP-AMPARs contributes to the enhanced synaptic dynamics in local inputs. (A and B) Enhanced or stable inward rectification of synaptic currents at local or long-range inputs, respectively, during postnatal maturation. (Left) Sample EPSCs under six holding potentials in PVNs (−80, −50, −20, +10, +40, and +70 mV) with averaged traces from 20 trials. (Right) Summaries of I–V curves by normalizing EPSC amplitude to that at −80 mV. (C) An example showing the effect of NAS, a blocker of CP-AMPARs, on basal transmission and synaptic dynamics at a local input (at P32). Basal transmission was tested by evoking single presynaptic APs (individual EPSCs are indicated by open circles). NAS (100 μM) was bath-applied at the indicated time. (Insets) EPSC 1 and 2 examined before and during NAS application; each trace was averaged from 20 trials. (D) Summary of synaptic dynamics at local inputs to PVNs during NAS application at young and mature ages. (E) Summaries of NAS effect on DI at the individual local inputs shown (D). The same connections are linked by a line. (F) DI change caused by NAS application. Open circles, individual inputs; filled circles, mean. (Error bars represent SEM; *P < 0.05, **P < 0.01, ***P < 0.001, Mann–Whitney test.)

with a high release probability (P_r) in presynaptic PyN terminals (20). We observed a low transmission failure rate at local inputs before P20 ($7.7 \pm 1.7\%$) and a significant increase in failure rate after P30 ($13.9 \pm 2.3\%$; $P = 0.03$). In parallel, there was a developmental increase in the variance of trial-by-trial uEPSC amplitude at local inputs quantified by the coefficient of variance (CV; 0.39 ± 0.02 before P20 vs. 0.50 ± 0.02 after P30, $P < 0.001$) (Fig. S10 A and B). These changes indicate a developmental reduction in either presynaptic P_r, the number of release sites, or both (21). We further used variance-mean (V-M) analysis to address this. V-M curves for local inputs were generated for a range of P_r by altering $Ca^{2+}:Mg^{2+}$ ratios in the perfusion solution (Fig. S11A). On graphical inspection (22) of V-M curves (Fig. S11B), a smaller degree of curvature was revealed in mature ages, indicating a decreased P_r in presynaptic PyN terminals. Considering the unchanged uEPSC amplitude (Table S1) with decreased P_r, an increase implies either the amount of postsynaptic receptors, the number of release sites, or both. Larger initial slopes in the V-M curve at the mature age suggest an increase of postsynaptic receptor. In contrast, no significant change was detected in the CV of uEPSC amplitude at long-range inputs (CV: 0.19 ± 0.02 vs. 0.20 ± 0.02, $P = 0.65$) (Fig. S10 C and D).

Polyamine-dependent facilitation of postsynaptic Ca^{2+}-permeable AMPA receptors (CP-AMPARs) can counteract short-term depression at excitatory synapses onto PVNs (23). The faster rise and decay times of uEPSCs at mature local inputs (Table S1) suggest an increased proportion of CP-AMPARs (24). CP-AMPAR–mediated current is typically inward-rectified due to the cytoplasmic polyamine block following membrane depolarization (25). We

from 0.54 ± 0.03 to 0.45 ± 0.04, $n = 8$, $P = 0.003$; Student's paired t test). The change of DI was significantly stronger at mature ages $(0.32 \pm 0.05$ vs. 0.09 ± 0.02, $P = 0.003)$ (Fig. 5 C–F). Taken together, we conclude that both presynaptic (decreased P_r) and postsynaptic (increased CP-AMPARs) changes contribute to the maturation of synaptic dynamics in local inputs to PVNs.

Discussion

Cortical parvalbumin interneurons are implicated in both feed-forward and recurrent inhibition (2). Direct optogenetic activation of PVNs strongly modulates PyN spiking and cortical gain control during visual processing and generates gamma oscillations that synchronize PyNs (9, 10). However, optogenetic manipulation bypasses endogenous physiological recruitment mechanisms. Whether PVNs are differentially recruited by afferent and local circuit activity is not well-understood. In fact, numerous studies (7, 8, 16, 17) demonstrate profound short-term synaptic depression of excitatory inputs onto PVNs, suggesting the puzzling notion that an inherently precise and robust PVN network appears poorly suited to follow the temporal dynamics of local circuits. Here we demonstrate synaptic recruitment of individual PVNs in V1 customized according to input sources with different maturation profiles. Whereas long-range inputs to PVNs retain short-term depression throughout juvenile to adult ages, local inputs progressively lose short-term depression.

Recent studies reveal a surprising degree of precision in inhibition recruited during network activity. For example, during sensory induced or spontaneously generated episodes of cortical activity, inhibition is often instantaneously and continuously correlated with excitatory inputs, and the magnitude of inhibition matches proportionally to excitation (26–28). PVNs show low input resistance and a high threshold for spiking (12, 29). Individual PVNs receive convergent inputs from local PyNs and in turn provide divergent reciprocal inhibition back to PyNs (30). Although excitatory input patterns that recruit PVNs are not well-characterized, they are likely activated by convergent inputs from multiple PyNs (8) that fire a burst of APs in response to sensory inputs (31) or during spontaneous alterations of cortical states (27). Therefore, little short-term depression at local inputs endows PVNs with exquisite sensitivity to the temporal patterns of local networks. This would facilitate a rapid and proportional transformation of input patterns to matching inhibition.

Conversely, long-range inputs recruit interneurons to produce short-latency inhibition that curtails synaptic excitation in principal cells (32). The short-term depression at these inputs would provide strong inhibition to principal cells at the onset of the AP series (33), thereby promoting gating and propagation of input signals with rapid onset and achieving effective gain modulation of input signals (34). Interestingly, neuronal responses in L2/3 of mouse V1 are strongly driven by locomotion and mismatches between actual and expected visual feedback (35). Our finding of direct M2 inputs to L2/3 PVNs in V1 might reveal a component of motor-related modulation of V1 processing.

A developmental decrease of short-term depression at local input synapses to PVNs has been reported in auditory cortex (36) and prefrontal cortex (37) during P16–P20, which is earlier than our findings in V1 (P20–P29). The maturation of inhibitory circuitry in mouse V1 is a prolonged process during which visual experience directs circuit wiring (38). Several studies have demonstrated significant maturation in intrinsic properties, inhibitory transmission, axon arbors, and innervation patterns of PVNs during the 2–3 wk after vision onset (11, 12). Therefore, a concerted maturation program appears to transform PVNs from a slow and inefficient signaling device to a sensitive, fast, and precise inhibitory network. Given this time course, the developmental enhancement of local inputs might represent another component of the PVN maturation program that regulates the critical period of ocular dominance plasticity (39).

What is the difference between local and long-range inputs to PVNs that might account for the differential dynamics and maturation profiles? One difference lies in their connectivity patterns: Local input sources (PyNs) receive reciprocal inhibition. Such inhibition is necessary to promote the maturation of local input dynamics. First, the maturation of PVN-to-PyN inhibitory transmission precedes the progressive loss of short-term depression at PyN-to-PVN synapses (Fig. 3B). Second, unidirectional PyN→PVN connections show a greater lack of maturation of temporal dynamics at mature ages than do reciprocal PyN⇌PVN pairs (Fig. 3D). Third, PyNs with reduced perisomatic inhibition (largely from PVNs) show more short-term depression at their synapses onto PVNs (Fig. 4).

How can PyNs distinguish PVNs that send feedback inhibition vs. those that do not and preferentially increase their excitatory synaptic dynamics onto PVNs with feedback inhibition? We suggest the following scenario. During the postnatal maturation of a PVN–PyN network, PVNs increase innervation by contacting more PyNs and making more synapses on each PyN (11). PVNs further form electrical coupling and reciprocal inhibitory connections among themselves, which promote synchronous firing of local PVN networks (5). PVN-mediated inhibition of PyNs and synchronous PVN networks may synergistically promote correlated activity between PyNs and PVNs through postinhibitory rebound or feedforward inhibition. It is possible that such correlated activities are required for the enhancement of PyN-to-PVN synaptic dynamics during development. Reciprocal PyN⇌PVN connections are more likely to achieve correlated activity with precise timing between presynaptic PyNs and postsynaptic PVNs than unidirectional PyN→PVN connections. This may account for the preferential enhancement of synaptic dynamics at PyN⇌PVN connections (Fig. 3E). In α1 knockdown, a reduction of PVN-mediated inhibition led to a further reduction of correlated activities at PyN→PVN connections formed by both α1-infected and naïve PyNs (Fig. 4 E and F). Because naïve PyN⇌PVN connections were unaffected by α1 knockdown (Fig. 4 C and D), together these results suggest that a threshold of sufficient correlated activity might enhance local input dynamics.

Recent studies indicate that PVNs show clear orientation tuning at eye opening but progressively lose this tuning during visual experience (40). The selective enhancement of local input dynamics might provide a potential explanation. The dominance of afferent inputs (which likely represent visual features) over local inputs likely confers orientation tuning at the time of eye opening, but the selective enhancement of local inputs would promote the summation of multiple excitatory inputs from PyNs with distinct and yet different tuning properties onto the same PVN, thereby erasing its initial orientation selectivity. More generally, the developmental stability of synaptic dynamics of long-range inputs to PVNs may reflect and reinforce the intrinsic global architecture of major neural pathways that link brain regions (e.g., those from M2 to V1), whereas the developmental malleability and maturation of local input dynamics allow activity patterns to shape PyN ensembles according to early experience.

Materials and Methods

Detailed information on materials and methods in this study is provided in *SI Materials and Methods*. Information on materials includes mouse strains and shRNA plasmids. Technical information on methods includes retrograde rabies tracing, CRACM and electrophysiology in brain slices, in utero electroporation, immunostaining, data analysis, and statistics.

NEUROSCIENCE

1. Markram H, et al. (2004) Interneurons of the neocortical inhibitory system. *Nat Rev Neurosci* 5(10):793–807.
2. Isaacson JS, Scanziani M (2011) How inhibition shapes cortical activity. *Neuron* 72(2):231–243.
3. Somogyi P, Tamás G, Lujan R, Buhl EH (1998) Salient features of synaptic organisation in the cerebral cortex. *Brain Res Brain Res Rev* 26(2-3):113–135.
4. Jonas P, Bischofberger J, Fricker D, Miles R (2004) Interneuron Diversity series: Fast in, fast out—Temporal and spatial signal processing in hippocampal interneurons. *Trends Neurosci* 27(1):30–40.
5. Galarreta M, Hestrin S (2001) Electrical synapses between GABA-releasing interneurons. *Nat Rev Neurosci* 2(6):425–433.
6. Bartos M, Vida I, Jonas P (2007) Synaptic mechanisms of synchronized gamma oscillations in inhibitory interneuron networks. *Nat Rev Neurosci* 8(1):45–56.
7. Yoshimura Y, Callaway EM (2005) Fine-scale specificity of cortical networks depends on inhibitory cell type and connectivity. *Nat Neurosci* 8(11):1552–1559.
8. Hofer SB, et al. (2011) Differential connectivity and response dynamics of excitatory and inhibitory neurons in visual cortex. *Nat Neurosci* 14(8):1045–1052.
9. Cardin JA, et al. (2009) Driving fast-spiking cells induces gamma rhythm and controls sensory responses. *Nature* 459(7247):663–667.
10. Atallah BV, Bruns W, Carandini M, Scanziani M (2012) Parvalbumin-expressing interneurons linearly transform cortical responses to visual stimuli. *Neuron* 73(1):159–170.
11. Chattopadhyaya B, et al. (2004) Experience and activity-dependent maturation of perisomatic GABAergic innervation in primary visual cortex during a postnatal critical period. *J Neurosci* 24(43):9598–9611.
12. Lazarus MS, Huang ZJ (2011) Distinct maturation profiles of perisomatic and dendritic targeting GABAergic interneurons in the mouse primary visual cortex during the critical period of ocular dominance plasticity. *J Neurophysiol* 106(2):775–787.
13. Miyamichi K, et al. (2011) Cortical representations of olfactory input by trans-synaptic tracing. *Nature* 472(7342):191–196.
14. Wall NR, Wickersham IR, Cetin A, De La Parra M, Callaway EM (2010) Monosynaptic circuit tracing in vivo through Cre-dependent targeting and complementation of modified rabies virus. *Proc Natl Acad Sci USA* 107(50):21848–21853.
15. Jackman SL, Beneduce BM, Drew IR, Regehr WG (2014) Achieving high-frequency optical control of synaptic transmission. *J Neurosci* 34(22):7704–7714.
16. Lu JT, Li CY, Zhao JP, Poo MM, Zhang XH (2007) Spike-timing-dependent plasticity of neocortical excitatory synapses on inhibitory interneurons depends on target cell type. *J Neurosci* 27(36):9711–9720.
17. Reyes A, et al. (1998) Target-cell-specific facilitation and depression in neocortical circuits. *Nat Neurosci* 1(4):279–285.
18. Doischer D, et al. (2008) Postnatal differentiation of basket cells from slow to fast signaling devices. *J Neurosci* 28(48):12956–12968.
19. Zucker RS, Regehr WG (2002) Short-term synaptic plasticity. *Annu Rev Physiol* 64:355–405.
20. Koester HJ, Johnston D (2005) Target cell-dependent normalization of transmitter release at neocortical synapses. *Science* 308(5723):863–866.
21. Bekkers JM, Stevens CF (1990) Presynaptic mechanism for long-term potentiation in the hippocampus. *Nature* 346(6286):724–729.
22. Clements JD, Silver RA (2000) Unveiling synaptic plasticity: A new graphical and analytical approach. *Trends Neurosci* 23(3):105–113.
23. Rozov A, Burnashev N (1999) Polyamine-dependent facilitation of postsynaptic AMPA receptors counteracts paired-pulse depression. *Nature* 401(6753):594–598.
24. Geiger JR, et al. (1995) Relative abundance of subunit mRNAs determines gating and Ca^{2+} permeability of AMPA receptors in principal neurons and interneurons in rat CNS. *Neuron* 15(1):193–204.
25. Bowie D, Mayer ML (1995) Inward rectification of both AMPA and kainate subtype glutamate receptors generated by polyamine-mediated ion channel block. *Neuron* 15(2):453–462.
26. Atallah BV, Scanziani M (2009) Instantaneous modulation of gamma oscillation frequency by balancing excitation with inhibition. *Neuron* 62(4):566–577.
27. Haider B, Duque A, Hasenstaub AR, McCormick DA (2006) Neocortical network activity in vivo is generated through a dynamic balance of excitation and inhibition. *J Neurosci* 26(17):4535–4545.
28. Okun M, Lampl I (2008) Instantaneous correlation of excitation and inhibition during ongoing and sensory-evoked activities. *Nat Neurosci* 11(5):535–537.
29. Cruikshank SJ, Lewis TJ, Connors BW (2007) Synaptic basis for intense thalamocortical activation of feedforward inhibitory cells in neocortex. *Nat Neurosci* 10(4):462–468.
30. Packer AM, Yuste R (2011) Dense, unspecific connectivity of neocortical parvalbumin-positive interneurons: A canonical microcircuit for inhibition? *J Neurosci* 31(37):13260–13271.
31. Haider B, et al. (2010) Synaptic and network mechanisms of sparse and reliable visual cortical activity during nonclassical receptive field stimulation. *Neuron* 65(1):107–121.
32. Pouille F, Scanziani M (2001) Enforcement of temporal fidelity in pyramidal cells by somatic feed-forward inhibition. *Science* 293(5532):1159–1163.
33. Pouille F, Scanziani M (2004) Routing of spike series by dynamic circuits in the hippocampus. *Nature* 429(6993):717–723.
34. Vogels TP, Abbott LF (2009) Gating multiple signals through detailed balance of excitation and inhibition in spiking networks. *Nat Neurosci* 12(4):483–491.
35. Keller GB, Bonhoeffer T, Hübener M (2012) Sensorimotor mismatch signals in primary visual cortex of the behaving mouse. *Neuron* 74(5):809–815.
36. Oswald AM, Reyes AD (2011) Development of inhibitory timescales in auditory cortex. *Cereb Cortex* 21(6):1351–1361.
37. Yang JM, Zhang J, Yu YQ, Duan S, Li XM (2014) Postnatal development of 2 microcircuits involving fast-spiking interneurons in the mouse prefrontal cortex. *Cereb Cortex* 24(1):98–109.
38. Huang ZJ, Di Cristo G, Ango F (2007) Development of GABA innervation in the cerebral and cerebellar cortices. *Nat Rev Neurosci* 8(9):673–686.
39. Levelt CN, Hübener M (2012) Critical-period plasticity in the visual cortex. *Annu Rev Neurosci* 35:309–330.
40. Kuhlman SJ, Tring E, Trachtenberg JT (2011) Fast-spiking interneurons have an initial orientation bias that is lost with vision. *Nat Neurosci* 14(9):1121–1123.